# Improvement of SI engine combustion with ammonia as fuel: Effect of ammonia dissociation prior to combustion

A. Mercier, Christine Mounaïm-Rousselle, Pierre Brequigny, J. Bouriot, C. Dumand

# Improvement of SI engine combustion with ammonia as fuel: effect of ammonia dissociation prior to combustion.

Authors: Mercier A[1]., Mounaïm-Rousselle C[1]., Brequigny P[1]., Bouriot J[2]., Dumand C[21]

## 1 Abstract:

Although recent studies have shown the possibility of running 'standard' spark-ignition engines with pure ammonia, the operating range remains limited mainly due to the unfavorable characteristics of ammonia for premixed combustion and often requires the addition of a complementary fuel such as $H_2$ to extend it. As the best way to add $H_2$ is to crack ammonia directly on-board, this paper focuses on the impact of the upstream cracking level of ammonia on the performance and emissions of a single cylinder spark ignition engine. Experiments were performed over several equivalence ratios, dissociation rates and load conditions. It is confirmed that only a slight rate of ammonia dissociation (10%) upstream of the combustion considerably enhances the engine's operating range thanks to a better combustion stability. In terms of pollutant emissions, the partial dissociation of ammonia, especially for slightly lean mixtures induces a very clear trade-off between high $NO_x$ and high unburned ammonia level for high and low ammonia dissociation rates, respectively. Therefore, cracking $NH_3$ does not only improve the operating range of ammonia-fueled spark ignition engines but can also help to reduce $NH_3$. However, to reach the same engine output work, higher ammonia fuel consumption will be necessary since the global system efficiency is lower using fuel dissociation. In addition, the global warming effect is increased with dissociation level since a higher level of $N_2O$ is generated by the hydrogen contribution.

Keywords: ammonia; hydrogen; dissociation; $NH_3$ cracking; e-fuel; combustion; internal combustion engine.

## 2 Nomenclature

[1]Laboratoire PRISME, Université d'Orléans, Orleans, France
[2]Innovation Department, STELLANTIS-PSA, Paris, France

| | |
|---|---|
| *SI* | Spark Ignition |
| CAD | Crank Angle Degree |
| *IMEP* | Indicated Mean Effective Pressure |
| *HRR* | Heat Release Rate |
| BMF | Burnt Mass Fraction |
| *CAXX* | CAD corresponding to XX% of FMB |
| *FTIR* | Fourier Transform Infrared |
| *SIT* | Spark Ignition Timing |
| *Pin* | Intake Pressure |
| *ISFC* | Indicated Specific Fuel Consumption |
| LBV | Laminar Burning Velocity |
| LHV | Lower Heating Value |
| COV | Covariance |
| NRJ | Energy |
| TDC | Top Dead Center |

## 3 Introduction

To be carbon neutral by 2050, the European Union needs to move away from fossil fuels as soon as possible. Using e-fuels such as ammonia and hydrogen for transportation can be part of the tools to reach this goal since their life cycle carbon footprint is low especially when they are produced from decarbonized sources [1–3]. Furthermore, a growing interest in ammonia has been observed in recent years as it has several advantages over hydrogen, namely: lower storage cost [4]; higher volumetric energy density; an existing and certified transport and storage network; and physical properties that simplify storage and transport. Recent studies have shown that it is possible to run a spark ignition (SI) engine using only ammonia as fuel over a wide operating range. In [2], an SI engine was run with using neat ammonia in a recent EP6 PSA SI Engine until 1bar of intake pressure guaranteeing less than 3% of $COV_{IMEP}$ and engine performances similar to those of methane. Despite satisfactory results at mid load, engine stability and combustion efficiency can be enhanced thanks to hydrogen addition [5,7]. However, in their study, Mounaïm-Rousselle *et al.* [8] indicated the limitations of pure ammonia combustion at low load for a SI engine. The minimum Indicated Mean Effective Pressure (IMEP) was limited to 5 bar using neat ammonia while 3 and 2 bars were reached with $H_2$ addition and a compression ratio increase respectively. Therefore, doping the engine with small amounts of hydrogen (5-10% by volume) or by increasing the compression ratio are two strategies that have been necessary so far to make the engine run stably at low load. The use of an on-board ammonia cracker can be seen

as a key to improving engine performance at low load for a low compression ratio engine. This was tested in [9] where it was shown that it is possible to start a cold engine with less than 10% hydrogen in the fuel in transient conditions. In [10], a numerical study provided an explanation for the effect of $NH_3$-dissociation on flame structure, combustion efficiency, maximum temperature and $NO_x$ emissions. It was found that $NO_x$ level increases when dissociating ammonia up to a dissociation level of 80% and then decreases until complete decomposition of the ammonia due to a decrease in maximum temperature at a very high dissociation level that limits the formation of thermal NO while fuel NO is no longer present. In addition, the same team concluded in [11] that by dissociating half of the $NH_3$ molecule, the Laminar Burning Velocity (LBV) of the fuel mixture can reach that of methane and the promoting effect of $H_2$ is much more significant than the inhibiting effect of $N_2$ even with a higher $H_2/N_2$ ratio than the one obtained naturally from dissociation. Finally, the effect of a dissociated ammonia blend with gasoline on engine performances using a real cracker was investigated in [12] and compared to ammonia/gasoline blend combustion without a catalyst in an SI engine. *Ryu et al.*[12] found 2 advantages of using an ammonia cracker: i) it promotes the engine combustion; ii) it reduces ammonia and $NO_x$ exhaust emissions, especially at low load due to the high conversion rate. However, it was impossible to maintain a constant dissociation rate when changing the ammonia flow rate and low conversion rates were used at high load due to a reduction of the residence time in the catalyst. Therefore, the present study reports new data on the effect of partial $NH_3$ dissociation on SI engine performances and exhaust polluting emissions. Eight different levels of dissociation were investigated (namely from 0 to 0.4, 0 corresponding to pure $NH_3$) and several loads in order to define what dissociation level would allow the best performances-polluting emissions trade-off for running an SI Engine. In addition, to support and better understand the findings, simulations were conducted with a zero-dimensional, two-zone Spark Ignition engine model of the CHEMKIN-PRO package in ANSYS, based on the NH3 reaction mechanism of Stagni *et al*. [13]. According to [11], this mechanism, which contains 31 species and 203 reactions, appears to be the most accurate to predict any chemical heat release and to highlight some tendencies of exhaust gases such as NO, $NO_2$, $N_2O$ and unburnt emissions ($NH_3$ and $H_2$).

## 4 Experimental setup

Engine experiments were conducted in a single cylinder SI engine, with the specifications indicated in Table 1. The geometry of the engine was modified, i.e. the stroke was increased from 85.8 mm to 115 mm in order to best match the engine architecture and the physical characteristics of ammonia. For this, a long stroke not only increases the volumetric ratio without changing the shape of the combustion chamber, thus keeping a constant surface/volume ratio at TDC but also increases the internal aerodynamics of the engine. A flat piston was implemented in this study to increase the compression ratio, as shown in Figure 1. The engine is driven by an electric motor at a various engine speeds. The main shaft is equipped with a Kubler optical encoder for angular position monitoring with a 0.1 Crank Angle Degree (CAD) resolution. A water-cooled AVL piezoelectric pressure transducer with a 0.1 CAD resolution provides in-cylinder pressure measurements. Its measuring range is 0 - 25 MPa. Engine intake and exhaust temperature and pressure are monitored using type K thermocouples and piezo-resistive absolute pressure transducers. The absolute cylinder pressure is obtained by equalizing the in-cylinder pressure and the mean absolute intake pressure ($P_{in}$), 20 CAD in the middle of the intake stroke. The spark plug used is the original one with a coil charging time set to 2 ms. For all the data presented below, several operating points were recorded with several Spark Ignition Timings (SIT). For each condition, the operating point with the maximum IMEP as control parameter that guarantees a $COV_{IMEP}$ below 5% was chosen. Ammonia, hydrogen (both 99.99% purity), nitrogen and air gaseous flows were measured and controlled using Brooks thermal mass flowmeters with +- 0.7% accuracy, preheated to the intake temperature of 323 K and premixed in an intake plenum prior to injection. A scheme of the experimental setup is shown in Figure 2.

*Table 1: Engine characteristics*

| | SI (EP6 LC) |
|---|---|
| Displaced volume(l) | 0.535 |
| Stroke (mm) | 115 |

| | |
|---|---|
| Bore (mm) | 77 |
| Connecting rod length (mm) | 177 |
| Compression ratio | 11.75 |
| Number of valves | 4 |
| Water and oil temperatures (°C) | 80 |

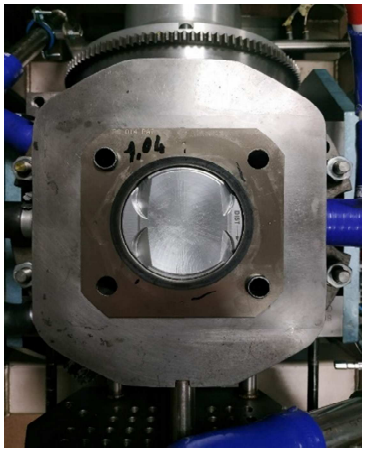

*Figure 1: Flat piston implemented for the study*

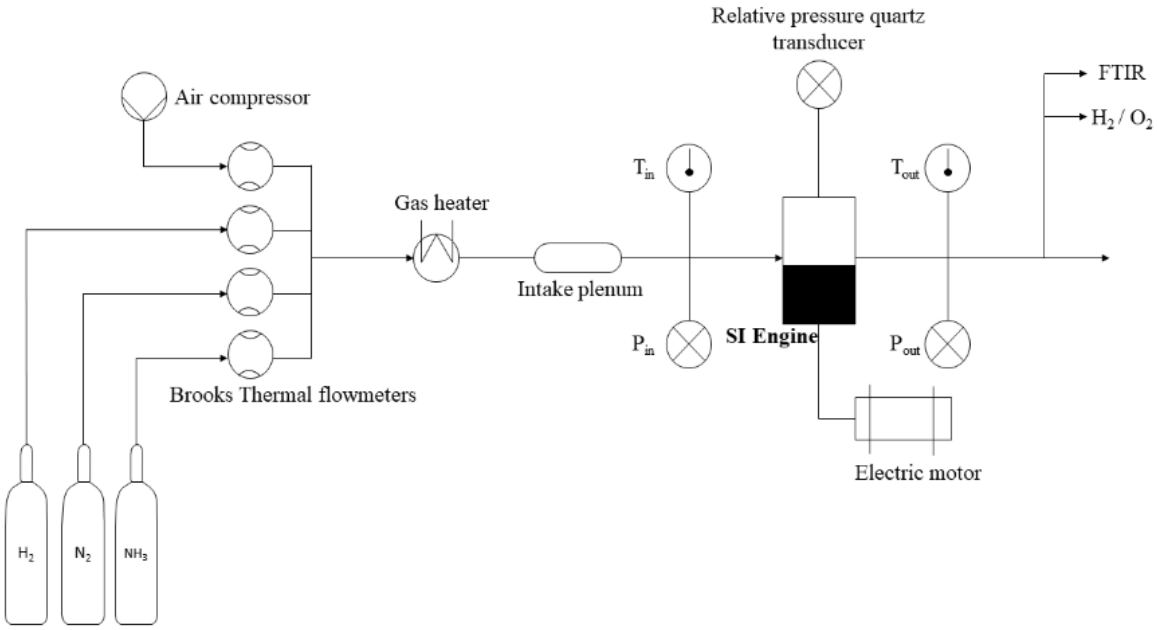


*Figure 2: Layout of the experimental setup*

98 The wet exhaust gases were analyzed using a Gasmet Fourier Transform Infrared (FTIR) spectrometer
99 to assess $H_2O$, NO, $NO_2$, and $NH_3$ concentrations. To obtain simultaneous quantitative measurement
100 of many gaseous species with a good time resolution and accuracy, the interferences between the
101 species of interest are correctly identified and considered in the analysis settings. The analysis ranges
102 of the species of interest can be found in Table (2). Lastly, $H_2$ exhaust measurement was performed
103 using a thermal conductivity gas sensor (XEN-5320), that determines the gas composition by
104 measuring the temperature elevation of a micromachined heater element. Its measurement range was
105 set to 0-10% in the case of ammonia combustion.

106 *Table 2: Analysis range settings to determine exhaust species concentration from FTIR*

| Species | Wave Length ($cm^{-1}$) |
|---|---|
| H2O | 3950 - 4240 |
| N2O | 2060 - 2280 |
| NO | 1850 - 2110 |
| NO2 | 2770 - 2990 |
| NH3 | 2990 - 3365 |

107 The apparent Heat Release Rate (HRR) was computed from pressure trace post processing with the
108 first law of thermodynamics, as follows:

109 $$\frac{dQ}{d\theta} = \frac{\gamma}{\gamma - 1} * P * \frac{dV}{d\theta} + \frac{1}{\gamma - 1} V * \frac{dP}{d\theta} \quad (1)$$

110 where $\gamma$ is the heat capacity ratio, P, V and $\theta$ , the cylinder pressure and volume and crank angle,
111 respectively. Note that heat losses are not considered in the calculation since they are very difficult to
112 determine; they will be the subject of future work. The Burnt Mass Fraction (BMF) is then obtained by
113 integrating the heat release and apparent HRR is then recalculated using the variable heat capacity
114 ratio computed from the previous BMF. The different phases of combustion propagation were
115 determined by estimating different characteristic timings, named CAXX, which are the Crank Angle
116 degrees corresponding to XX% of the burnt mass fraction. The CA10, CA50 and CA90 are also used

as input data, for the built-in zero-dimensional, two-zone SI engine model in Chemkin Pro, to determine the best-fit Wiebe function, since the mass is transferred between the 2 zones at the rate and timing specified by the Wiebe function. In addition, The Woshni wall heat exchange model was used to estimate the energy fraction lost at the wall and the convection coefficient was optimized by changing only the $C_0$ value from Equation (2) until Equation (3) becomes true. Due to high modelling uncertainties the CAXX plotted in the present study were computed using apparent heat release.

$$h_c = C_0 \left( B^{-0,2} P_{Cyl}^{0,8} \left( (C_1 C_m) + \frac{C_2 C_u T_{BDC}}{P_{BDC} V_{BDC}} \left( P_{cyl_{(\theta)}} - P_{0_{(\theta)}} \right) \right)^{0,8} T_{Cyl}^{-0,53} \right) \quad (2)$$

$$\int_{SIT}^{CA90} dQ_{Comb} = 0,9 * m_{fuel} * LHV_{fuel} * \eta_{Comb} \quad (3)$$

## 4.1 Operating conditions

Assuming that ammonia can be dissociated in hydrogen and nitrogen by means of an on-board cracker, molar fractions of each species were defined following Equation (4), i.e. considering a constant mass; this differs from [11] where a constant volume was chosen. In addition, $NH_3$ dissociation upstream of the combustion chamber was simulated on the test bench through flowmeters as schematized in Figure 2.

$$\alpha NH_3 + (1-\alpha)\left(\frac{3}{2}H_2 + \frac{1}{2}N_2\right) + \frac{3}{4}(O_2 + 3.78N_2) \rightarrow \frac{3}{2}H_2O + \left(\frac{1}{2} + \frac{3}{4} * 3.78\right)N_2 \quad (4)$$

Therefore, the α coefficient represents the molar fraction of $NH_3$ that is not dissociated and can be defined as follows:

$$\alpha = \frac{\frac{3}{2} * X_{NH3}}{\frac{3}{2} * X_{NH3} + X_{H2}} \quad (5)$$

with $X$ the molar fraction of each species in the fuel. All operating conditions are summarized in Table 3.

For each operating condition, a Spark Ignition Timing (SIT) sweep was performed in order to find the optimal CA50 phasing for each blend. The criterion depends on both combustion stability and the best IMEP. From the equivalence ratio definition (Equation (6)), three different levels (0.9, 1 and 1.1) were investigated. All of them are close to stoichiometry in order to see the impact of mixture composition on covariance and polluting emissions without having very high levels of $NO_x$ and $NH_3$ for lean and rich conditions, respectively. Therefore, to keep both equivalence ratio and intake pressure constant, volumetric air and fuel flows were adjusted as a function of the dissociation level.

$$\phi = \frac{(\dot{V}_{H2} + \dot{V}_{NH3})}{\dot{V}_{air}} * AFR_{stoe_{vol}} \quad (6)$$

with $AFR_{stoe}$, the volumetric stoichiometric air/fuel ratio.

*Table 3: Engine operating conditions*

| | |
|---|---|
| Engine speed (rpm) | 1000 |
| Intake temperature (°C) | 50 |
| Intake pressure (bar) | [1; 0.8; minimum] |
| $\phi$ (-) | [0.9; 1; 1.1] |
| $\alpha_{NH3}$ | [1; 0.98; 0.95; 0.9; 0.85; 0.8; 0.7; 0.6] |

Table 4 sums up the Lower Heating Value (LHV) by mass and mole for 100 and 0% of cracked ammonia and for neat hydrogen for comparison, to highlight the decrease in energy in the case of a full dissociation of ammonia due to the presence of nitrogen. Indeed, although the LHV per mixture increases with the increase in hydrogen content, if the nitrogen is kept, the volumetric energy density drops a slighlty with the level of dissociation, namely -6% between neat ammonia and fully decomposed ammonia.

155 *Table 4: Mixture LHV comparison between neat ammonia, neat hydrogen and dissociated ammonia at $\phi = 1$*

| $\boldsymbol{\phi = 1}$ | LHV per mixture mass (kJ/kg) | LHV per mixture mol (kJ/mol) |
|---|---|---|
| α=1 (Neat $NH_3$) | 2643 | 69.31 |
| α=0 ($H_2$+$N_2$) | 3026 | 65.11 |
| Neat $H_2$ | 3427 | 71.53 |

156

157 Figure 3.a) highlights the effect of $NH_3$ cracking on the mixture energy content – by mass and volume
158 –, mixture density and introduced energy relative to the value obtained in the neat ammonia condition
159 for all tested dissociation levels assuming once again that nitrogen is kept in the mixture. Mass and
160 volume energy content behave in an opposite way due to the very low density of hydrogen. Therefore,
161 as the filling efficiency does not change much (only subject to intake temperature variations), the
162 energy content introduced in the engine – derived from the flow meters – drops as the $NH_3$
163 dissociation level increases. However, by using the optimized Goldmann and Dinkelacker semi
164 empirical correlation given in [14], it can be seen that the increase of nitrogen in the mixture as a
165 function of dissociation level will not compensate the Laminar Burning Velocity (LBV) increase as
166 plotted in Figure 3.b), where conditions at SIT for in-cylinder pressure and temperature were chosen
167 as initial conditions for the calculation.

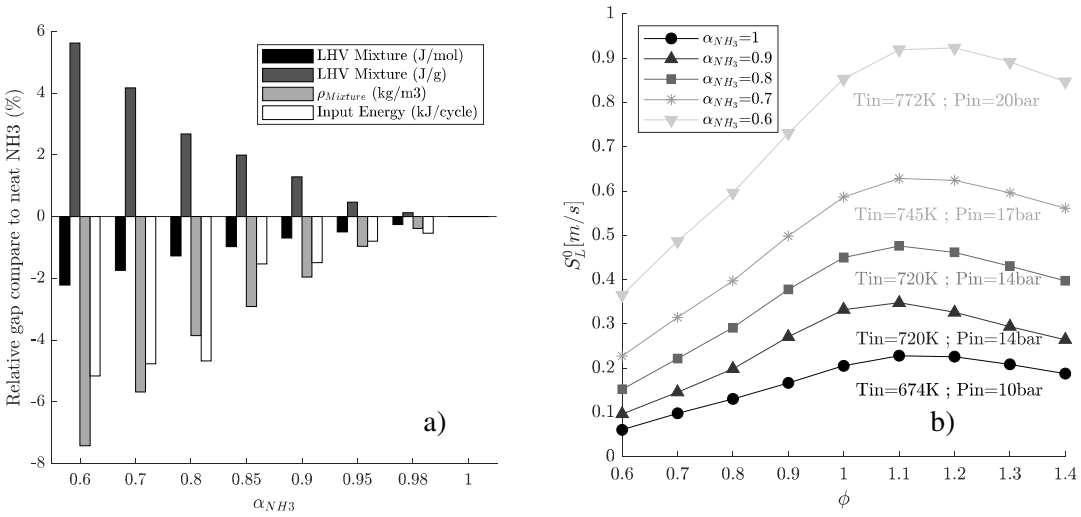


*Figure 3: a) Relative effect of dissociation on mixture LHV and Input Energy; b) Dissociation effect on Laminar Burning Velocity from semi-empirical correlation [14].*

# 5 Results and discussion

## 5.1 $NH_3$-dissociation effect on engine performances

All the results presented in section 5.1 and 5.2 were performed at a constant intake pressure of 1 bar and 1000 rpm. Since the energy mixture content is higher in neat $NH_3$ conditions, due to the energy molar density, for a constant intake pressure and equivalence ratio, IMEP is as expected higher as shown in Figure 4.a and therefore decreases as a function of dissociation level. The effect is less significant for slightly lean air/fuel mixtures, i.e. less than 3% for $\phi = 0.9$ in comparison to 6% for $\phi = 1.1$. Furthermore, as indicated, efficiency is relatively constant: the decrease of IMEP is of the same order of magnitude as the decrease in energy content (Figure 3a).

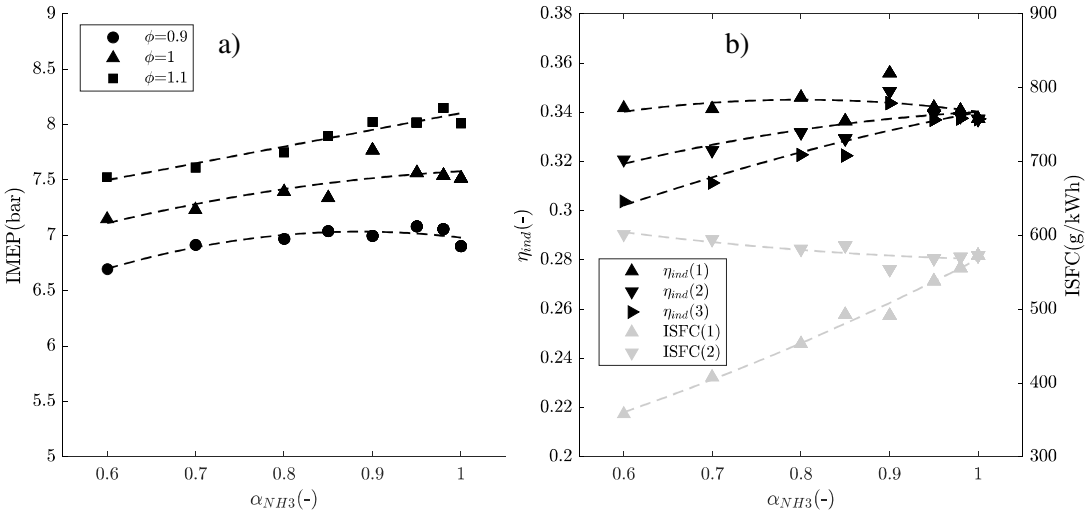


*Figure 4: a) Dissociation effect on IMEP and ISFC for several equivalence ratios at 1000rpm and 1bar; b) Comparison of engine indicated efficiency and global (engine + cracker) efficiency as a function of dissociation level at $\phi = 1$, 1bar and 1000 rpm.*

However, when the LHV loss due to partial $NH_3$ decomposition is considered, as explained in Equations (6,7), the indicated efficiency drops much more with the increase in dissociation rate (-4% at $\alpha_{NH3} = 0.8$). On the other hand, by considering Equation (9), Indicated Specific Fuel Consumption (ISFC) is no longer a reflection of the indicated efficiency since the LHV of the fuel changes as the degree of dissociation varies except if the neat ammonia condition is taken as a reference (Equation (10)). The way of calculating the engine efficiency in Equation (6) is interesting to understand the fundamental aspects of combustion while Equation (7) is better adapted to a system approach, i.e. with an ammonia tank and an on-board cracker. Moreover, if the external energy requirement to decompose $NH_3$ ($NH_3$ cracking NRJ presented in Equation (11)) is considered, the efficiency of the engine drops even more as the dissociation level increases, i.e. -2.3 % at $\alpha_{NH3} = 0.8$ (Equation (8)).

$$\eta_{ind_{(1)}} = \frac{W_i}{\left(m_{fuel} * LHV_{fuel}\right)_{post_{cracker}}} \quad (6)$$

$$\eta_{ind_{(2)}} = \frac{W_i}{\left(m_{fuel} * LHV_{fuel}\right)_{before_{cracker}}} \quad (7)$$

$$\eta_{ind_{(3)}} = \frac{W_i}{\left(m_{fuel} * LHV_{fuel}\right)_{before_{cracker}} + NH_{3_{cracking_{NRJ}}}} \quad (8)$$

$$ISFC_1 = \frac{\left(\dot{m}_{fuel}\right)_{post_{cracker}}}{Power_i} \quad (9)$$

$$ISFC_2 = \frac{\left(\dot{m}_{fuel}\right)_{before_{cracker}}}{Power_i} \quad (10)$$

$$NH_{3_{cracking_{NRJ}}} = \left(1 - \alpha_{NH_3}\right) * \Delta H^0_{f(298)} * X_{NH_{3_{mixture}}} * \frac{Tot_{VFR} * 2}{22.4 * N} \quad (11)$$

with $X_{NH_{3_{mixture}}}$ the molar fraction of ammonia in the mixture and $Tot_{VFR}$ the total volumetric flow rate in NL/min.

$$\eta_{comb} = 1 - \frac{Q_{unburnt}}{Q_{fuel}} = 1 - \frac{\dot{m}_{H_2} * LHV_{H_2} + \dot{m}_{NH_3} * LHV_{NH_3}}{\dot{m}_{fuel} * LHV_{fuel}} \quad (12)$$

$$\eta_{thermo} = 1 - \frac{1}{CR^{\gamma-1}} \quad (13)$$

$$\eta_{shape} = \frac{\eta_{ind}}{\eta_{comb} * \eta_{thermo}} \quad (14)$$

Efficiency details are given in Figure 5.a and formulas in Equations (12), (13) and (14), where the combustion efficiency ( $\eta_{comb}$) is improved by dissociating ammonia due to a lower combustion duration. This is also highlighted in Figure 6.b. It is induced by the laminar burning velocity and the flame temperature increase, in accordance with [7]. One can assume that engine stability does not affect combustion efficiency since at optimal SIT, it always remains under 2% of $COV_{IMEP}$ (for intake pressure of 1 bar) as shown in Figure 5.b. On the other hand, the adiabatic constant, $\frac{Cp}{Cv}$ ratio linearly drops slighlty bit in neat ammonia conditions leading to a decrease in theoretical thermodynamic efficiency ($\eta_{th}$) since the compression ratio is fixed. Finally, the reduction of combustion duration due to the laminar burning velocity increase when dissociating $NH_3$ leads to a Spark Ignition Timing (SIT) adjustment in order to get the best IMEP as explained in Section 4. The wall heat exchanges noted XWall and represented in Figure 5.b is defined as the ratio between the calculated energy lost at the wall and the engine input energy. It increases with dissociation due to the maximim Heat Release Rate

(HRR) increase, leading to a global decrease in shape efficiency ($\eta_{shape}$) with dissociation. In addition, optimal SIT is reduced by increasing the dissociation level due a decrease in both ignition delay and combustion duration noted CA10-SIT and CA90-CA10 as can be seen in Figure 6.a and b respectively.

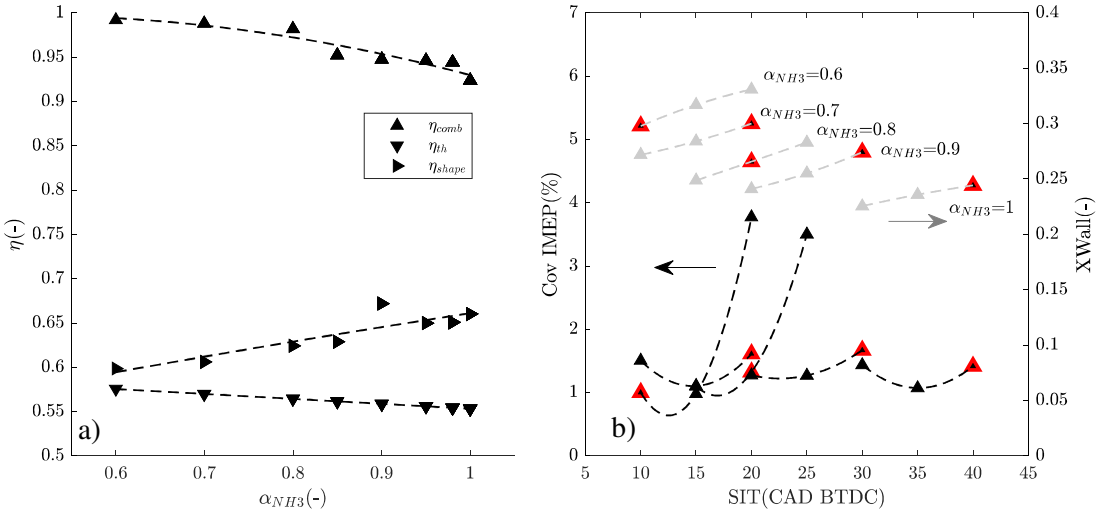


*Figure 5: a) Effect of $NH_3$ dissociation on efficiencies at $\phi = 1$, 1bar and 1000 rpm; b) Wall energy lost fraction as a function of SIT for several dissociation levels. Optimized SIT is colored in red.*

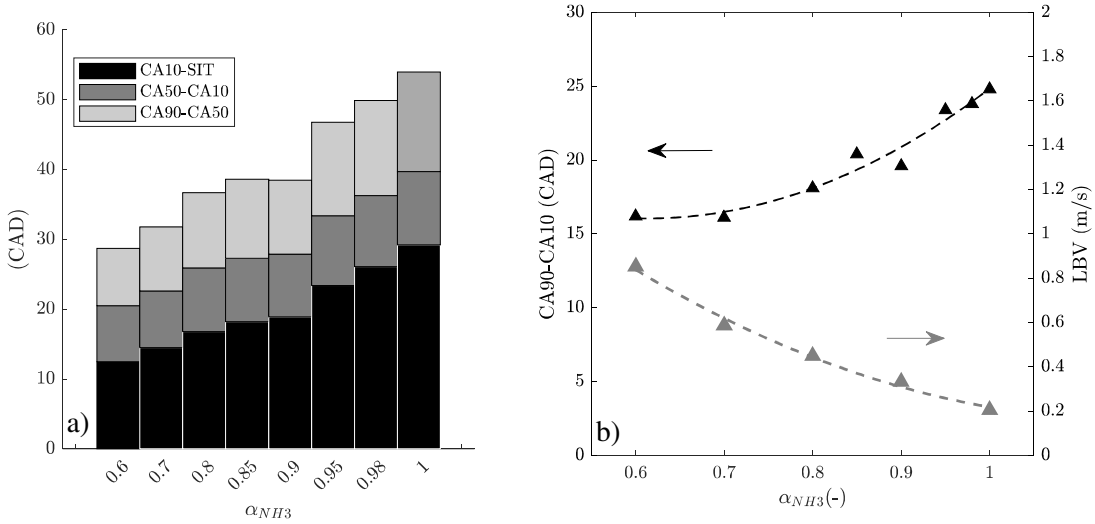


*Figure 6: a) Durations of different phases of combustion development as a function of dissociation level at 1bar, 1000 rpm and $\phi = 1$; b) correlation between computed LBV and full combustion duration at 1bar and 100 0rpm.*

## 5.2 $NH_3$-dissociation effect on engine pollutant emissions

In Figures 7.a), $NO_x$ emissions are presented. Both the dissociation level and the equivalence ratio strongly affect these emissions. The difference between the $NO_x$ level at $\phi = 1.1$ and $\phi = 1$ increases when the dissociation degree is increased. As the $NO_x$ level increases following the amount of $H_2$ content in the fuel and both thermal and fuel $NO_x$ depend on temperature, this means that $NO_{x\_thermal}$ increases faster than $NO_{x\_fuel}$ drops. However, the results from the 0D simulation indicate that the ratio between $NO_{x\_thermal}$ and $NO_{x\_total}$ remains around 80% regardless of the level of dissociation so that $NO_x$ formation is mainly governed by Equation (15) of the Zeldovich mechanism. Furthermore, Figures 7.c and 7.d show that a very good agreement can be observed, up to 15% of dissociation, between simulated and measured $NO_x$ and $N_2O$ emission trends at the end of the cycle where almost all $NO_x$ produced during the combustion process are released at the exhaust (Figure 7.b). Also, as already shown in previous studies [15], $NO_x$ are mainly composed of NO. Finally, the $NO_x$ level obtained in neat ammonia combustion at $\phi = 0.9$ is very close to the one measured in [5] (namely 1% higher) in the case of methane combustion for a similar engine type and operating conditions, which is a very positive point for the feasibility of a $NO_x$ aftertreatment system.

$$Zeldovich\ Mechanism:$$

$$N + NO \Leftrightarrow O + N_2 \quad (15)$$

$$N + OH \Leftrightarrow NO + H \quad (16)$$

$$N + O_2 \Leftrightarrow NO + O \quad (17)$$

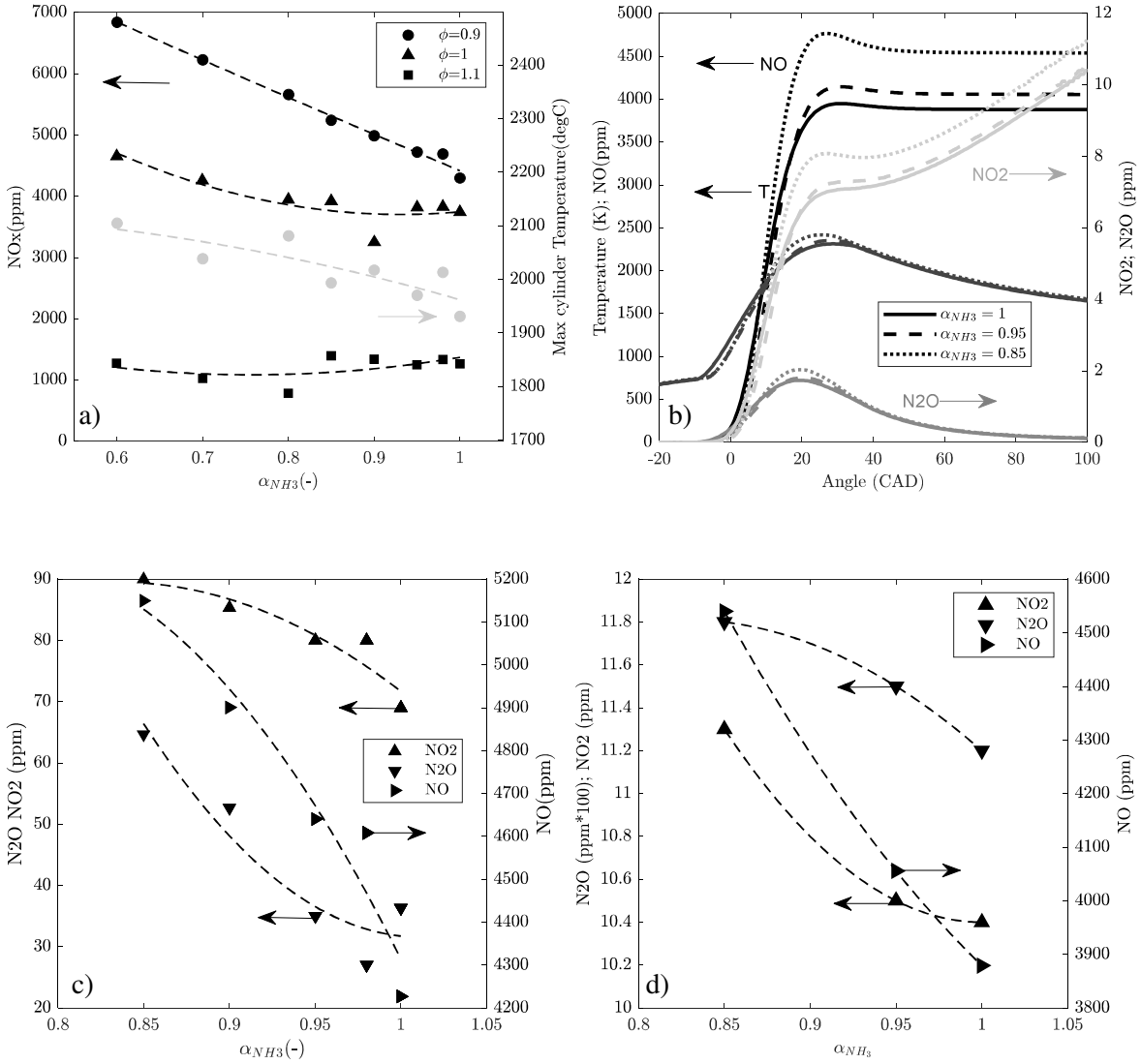


*Figure 7: NOx and $N_2O$ emissions a) $NO_x$ emissions and maximum in-cylinder temperature as a function of dissociation degree and equivalence ratio – Pin= 1bar and 1000 rpm; b) NO, $NO_2$, $N_2O$ and in-cylinder temperature trend from chemical kinetic simulation for 3 different dissociation levels; c) Measured exhaust emissions; d) Simulated exhaust emissions. $\phi$ = 0.9, Pin = 1bar and 1000 rpm for b) c) and d)*

$N_2O$ emissions are higher at high dissociation levels where NO concentration is also high. Therefore, since $NH_3$ remains the major fuel species, one can assume that the high temperature $N_2O$ pathway is dominant in the present case study (Equation (18)) since NO is dominant species in $NO_x$ emissions as explained in [15]. However, based on the kinetic mechanism, the latter pathway occurs mainly the reverse direction, meaning that part of the $N_2O$ is dissociated into NO and not the contrary. Thus, the $N_2O$ production rate is likely mainly governed by Equations (19) and (20), where production is spread equally over the two pathways as shown in Figure 8.

263

264 $$NH + NO \Leftrightarrow N_2O + H \quad (18)$$

265 $$N_2O(+M) \Leftrightarrow N_2 + O(+M) \quad (19)$$

266 $$N_2O + H \Leftrightarrow N_2 + OH \quad (20)$$

267

268

269 The above explanations and Figure 8 confirm that the dissociation effect promotes the occurrence of
270 $NO_2$ NO and $N_2O$. Indeed, Figure 8 indicates that even though more $N_2O$ is dissociated (Equation
271 (18)) at $\alpha_{NH_3} = 0.85$, more N2O is also formed (see Equation (19) and (20) resulting in a very slight
272 increase in $N_2O$ emissions as presented in Figure 7.b, c and d.

273

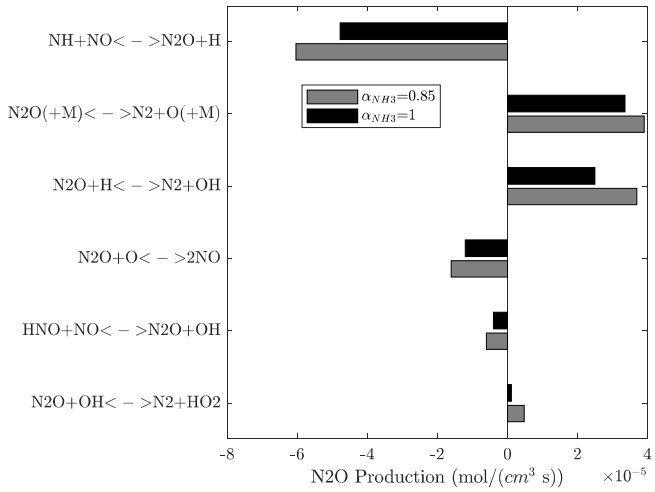


274

275 *Figure 8: $N_2O$ production reaction pathway at the maximum production rate for 1000 rpm, 1bar.*

276

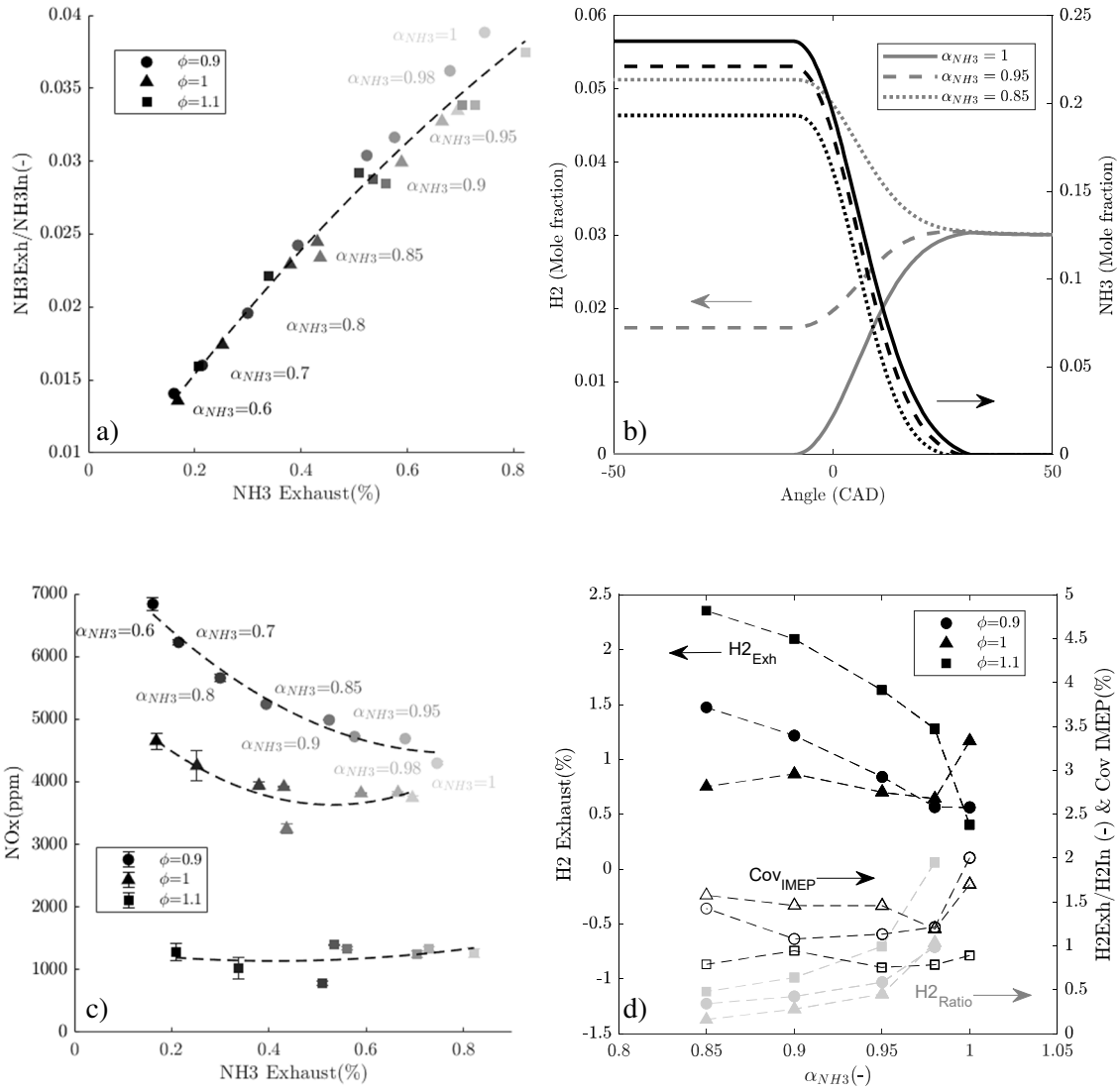


*Figure 9: Unburnt fuel emissions a) Ratio between intake and exhaust $NH_3$ mass flow rate as a function of exhaust NH3 concentration for several $\phi$ and $\alpha_{NH3}$; b) example of ammonia and hydrogen molar fraction as a function of crank angle degree at $\phi = 1.1$ for 3 dissociation levels, obtained by simulation; c) $NO_x$ vs $NH_3$ trade-off; d) Ratio between intake and exhaust hydrogen mass flow rate and exhaust hydrogen concentration as a function of dissociation level and equivalence ratio. Pin= 1bar and 1000 rpm.*

As mentioned earlier, ammonia dissociation enhances combustion due to H2 production, thus improving combustion efficiency. Therefore, in the case of ammonia combustion both H2 and NH3 species are present at the exhaust. Logically, higher quantity of ammonia and hydrogen are found for low and high dissociation levels, respectively, following the amount of H2 and NH3 at the intake. The combustion is very stable for every operating point at 1bar of intake pressure and 1000rpm, as shown in figure 9.d). The $COV_{IMEP}$ always remains under 2% or even lower in slightly rich mixtures, a trend

also observed in [8]. Ammonia emissions did not change significantly with the change in air/fuel ratio, namely +17% and +6% in lean and rich mixtures due to the combustion stability problem and excess fuel respectively. This means that most of the measured ammonia might come from the crevice mechanism proposed by Westlye et al. [15] (Dead volumes in which the air/fuel mixture is present but cannot be burned because the flame cannot propagate).

On the other hand, hydrogen exhaust emissions illustrated in Figure 9.d) increase with the equivalence ratio, especially for a high dissociation level (+200% at $\alpha_{NH3} = 0.85$). This confirms that most of the fuel which is not trapped might be converted into $H_2$, as predicted by the 0D simulation and presented in Figure 9.b where 3% of hydrogen is found at the exhaust and the $NH_3$ level is almost zero. However, this trend is no longer true experimentally in the case of neat ammonia combustion where the hydrogen exhaust level is constant as a function of the equivalence ratio while, as already mentioned, the ammonia exhaust measurement increases by 20% between stochiometric and slightly rich mixtures ($\phi = 1.1$). In slightly rich mixtures, trapped ammonia increases sufficiently to impact the corrected equivalence ratio ($\phi_{cor}$) presented in Equation (21). Its value drops by 5% and reaches a value of 1.05, meaning that a lower level unburnt $H_2$ level is expected at the exhaust. This could explain why hydrogen remains constant for neat ammonia operating conditions as a function of the equivalence ratio if all exhaust ammonia is considered as trapped ammonia.

$$\phi_{cor} = \frac{\dot{m}_{fuel} - \dot{m}_{NH_{3(trapped)}}}{\dot{m}_{air}} * AFR_{stoe_{mass}} \quad (21)$$

On the other hand, relative to the amount of hydrogen at the intake, $H_2$ emissions turn out to be larger in neat ammonia combustion, as shown in Figure 9.d, following the combustion efficiency evolution. As a result, 15% of ammonia dissociation can reduce the unburnt $NH_3$ emissions by a factor 2 whatever the equivalence ratio. Figure 9.c shows a clear tradeoff between $NO_x$ and $NH_3$ in lean and in stoichiometric mixture as a function of the dissociation level. For a slightly rich mixture, since $NO_x$ emissions are very low, the level is no longer affected by dissociation contrary to $NH_3$ emissions.

As a result, $NO_x$ emissions were strongly reduced by adjusting the equivalence ratio: for example, a decrease of 70% or 80% from $\phi = 0.9$ to 1.1, for $\alpha_{NH3} = 1$ or $\alpha_{NH3} = 0.6$ respectively, while ammonia emissions could be managed by using dissociation level, giving a decrease of 100% from $\alpha_{NH3} = 1$ to $\alpha_{NH3} = 0.6$ whatever the equivalence ratio.

### 5.3 Low load operating range extension

The use of ammonia cracking is also one means to extend the low load operating condition range of the engine as highlighted in Figure 10.a. The stability criterion, i.e. 5% of IMEP covariance is reached for lower and lower inlet pressures as the dissociation level increases. Keeping 85% of ammonia in the fuel provides around 2 bars of IMEP, namely the same value as in a high compression ratio engine [8], which is near to engine output work at idle condition. The intake pressure map (Figure10.b) globally indicates once again the advantage of running the engine in a slightly rich mixture to guarantee stable condition at low load.

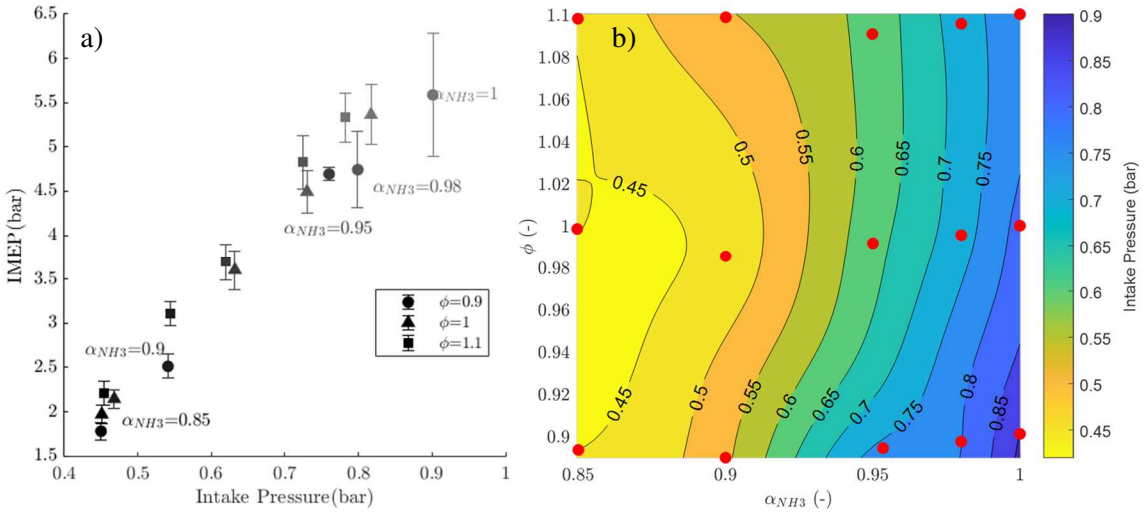


*Figure 10: a) minimum IMEP vs minimum intake pressure at 1000rpm and Cov IMEP<5% showed through error bars as a function of both equivalence ratio and dissociation level; b) minimum intake pressure MAP as a function of both equivalence ratio and dissociation level.*

.

## 6 Conclusion

The present study has focused on the potential effect of ammonia dissociation on SI engine performances and exhaust emissions in steady state conditions where both hydrogen and nitrogen were kept in the mixture after ammonia dissociation. Firstly, this study shows that cracking ammonia reduces the mixture energy content at the intake and therefore the energy output. Despite a constant indicated efficiency where combustion efficiency improvement is globally balanced by higher wall heat losses, the global efficiency is reduced due to a drop in the fuel Lower Heating Value and even more if the energy required to dissociate ammonia is considered. Secondly as the dissociation enhances combustion efficiency, it reduces unburnt ammonia emissions at the expense of hydrogen emissions, which increase in absolute value. Even though the hydrogen level remains under 2% in the exhaust emissions, it has to be considered since recent studies showed the potential indirect global warming effect of hydrogen [16]. The N2O level also has to be considered since it doubles when dissociating 15% of upstream ammonia, reaching 60 ppm, which represents roughly 1.5% of CO2, therefore doubling the greenhouse gas emissions without counting the indirect effect of the H2 previously mentioned. This study confirms that the best equivalence ratio to run the engine is a slightly rich once since low NOx are emitted and unburnt ammonia is mainly due to trapped ammonia. NOx emissions could be strongly reduced by adjusting the equivalence ratio, while ammonia emissions could be managed by adapting the dissociation level and are not significantly impacted by the equivalence ratio. Finally, as expected, even with a small fraction of nitrogen in the mixture, ammonia cracking improves combustion stability and extends the operating range of the engine at low load, i.e., achieving low-load operating conditions similar to those of a high-compression ratio engine (of the spark-ignition assisted diesel type [8]). However, there is much less unburned ammonia due to the optimized engine geometry for premixed combustion.

## 7 Acknowledgements

This project received support from the European Union's Horizon 2020 research and innovation program under grant agreement No. 862482 (ARENHA project).

# 8 References


[1] Vezina G, Bicer Y, Dincer I, Zamfirescu C, Raso F. Key Life Cycle Assessment Numbers for NH3 , Green and Brown Energy 2016.

[2] Boero AJ, Kardux K, Kovaleva M, Salas DA, Mooijer J, Mashruk S, et al. Environmental life cycle assessment of ammonia-based electricity. Energies 2021;14. https://doi.org/10.3390/en14206721.

[3] Bicer Y, Dincer I. Life cycle assessment of ammonia utilization in city transportation and power generation. J Clean Prod 2018;170:1594–601. https://doi.org/10.1016/j.jclepro.2017.09.243.

[4] Valera-Medina A, Amer-Hatem F, Azad AK, Dedoussi IC, De Joannon M, Fernandes RX, et al. Review on ammonia as a potential fuel: From synthesis to economics. Energy and Fuels 2021;35:6964–7029. https://doi.org/10.1021/acs.energyfuels.0c03685.

[5] Lhuillier C, Brequigny P, Contino F, Rousselle C. Combustion Characteristics of Ammonia in a Modern Spark-Ignition Engine. SAE Tech Pap 2019. https://doi.org/10.4271/2019-24-0237.

[6] Koike M, Suzuoki T. In-line adsorption system for reducing cold-start ammonia emissions from engines fueled with ammonia and hydrogen. Int J Hydrogen Energy 2019;44:32271–9. https://doi.org/10.1016/j.ijhydene.2019.10.105.

[7] Lhuillier C, Brequigny P, Contino F, Rousselle C. Performance and Emissions of an Ammonia-Fueled SI Engine with Hydrogen Enrichment. SAE Tech Pap 2019;2019-Septe. https://doi.org/10.4271/2019-24-0137.

[8] Mounaïm-Rousselle C, Mercier A, Brequigny P, Dumand C, Bouriot J, Houillé S. Performance of ammonia fuel in a spark assisted compression Ignition engine. Int J Engine Res 2021:1–12. https://doi.org/10.1177/14680874211038726.

[9] Koike M, Suzuoki T, Takeuchi T, Homma T, Hariu S, Takeuchi Y. Cold-start performance of an ammonia-fueled spark ignition engine with an on-board fuel reformer. Int J Hydrogen

Energy 2021;46:25689–98. https://doi.org/10.1016/j.ijhydene.2021.05.052.

[10] Wang Z, Ji C, Wang D, Hou R, Zhang T, Wang S. Experimental and numerical study on premixed partially dissociated ammonia mixtures. Part II: Numerical study of premixed combustion characteristics. Fuel 2021;306:121660. https://doi.org/10.1016/J.FUEL.2021.121660.

[11] Ji C, Wang Z, Wang D, Hou R, Zhang T, Wang S. Experimental and numerical study on premixed partially dissociated ammonia mixtures. Part I: Laminar burning velocity of NH3/H2/N2/air mixtures. Int J Hydrogen Energy 2021. https://doi.org/10.1016/j.ijhydene.2021.10.269.

[12] Ryu K, Zacharakis-Jutz GE, Kong SC. Performance enhancement of ammonia-fueled engine by using dissociation catalyst for hydrogen generation. Int J Hydrogen Energy 2014;39:2390–8. https://doi.org/10.1016/j.ijhydene.2013.11.098.

[13] Stagni A, Cavallotti C, Arunthanayothin S, Song Y, Herbinet O, Battin-Leclerc F, et al. An experimental, theoretical and kinetic-modeling study of the gas-phase oxidation of ammonia. React Chem Eng 2020;5:696–711. https://doi.org/10.1039/c9re00429g.

[14] Lhuillier C, Brequigny P, Lamoureux N, Contino F, Mounaïm-Rousselle C. Experimental investigation on laminar burning velocities of ammonia/hydrogen/air mixtures at elevated temperatures. Fuel 2020;263. https://doi.org/10.1016/j.fuel.2019.116653.

[15] Westlye FR, Ivarsson A, Schramm J. Experimental investigation of nitrogen based emissions from an ammonia fueled SI-engine. Fuel 2013;111:239–47. https://doi.org/10.1016/j.fuel.2013.03.055.

[16] Sand M, Myhre G, Sandstad M, Skeie RB. Atmospheric Impacts of Hydrogen as an Energy Carrier, 2020.